

RESEARCH

Open Access



Construction of a comprehensive predictive model for axillary lymph node metastasis in breast cancer: a retrospective study

Yan Li¹, Dong Han¹, Cong Shen¹ and Xiaoyi Duan^{1*}

Abstract

Purpose The accurate assessment of axillary lymph node metastasis (LNM) in early-stage breast cancer (BC) is of great importance. This study aimed to construct an integrated model based on clinicopathology, ultrasound, PET/CT, and PET radiomics for predicting axillary LNM in early stage of BC.

Materials and methods 124 BC patients who underwent 18 F-fluorodeoxyglucose (18 F-FDG) PET/CT and whose diagnosis were confirmed by surgical pathology were retrospectively analyzed and included in this study. Ultrasound, PET and clinicopathological features of all patients were analyzed, and PET radiomics features were extracted to establish an ultrasound model (clinicopathology and ultrasound; model 1), a PET model (clinicopathology, ultrasound, and PET; model 2), and a comprehensive model (clinicopathology, ultrasound, PET, and radiomics; model 3), and the diagnostic efficacy of each model was evaluated and compared.

Results The T stage, US_BIRADS, US_LNM, and PET_LNM in the positive axillary LNM group was significantly higher than that of in the negative LNM group ($P=0.013$, $P=0.049$, $P<0.001$, $P<0.001$, respectively). Radiomics score for predicting LNM (RS_LNM) for the negative LNM and positive LNM were statistically significant difference (-1.090 ± 0.448 vs. -0.693 ± 0.344 , $t = -4.720$, $P<0.001$), and the AUC was 0.767 (95% CI: 0.674–0.861). The ROC curves showed that model 3 outperformed model 1 for the sensitivity (model 3 vs. model 1, 82.86% vs. 48.57%), and outperformed model 2 for the specificity (model 3 vs. model 2, 82.02% vs. 68.54%) in the prediction of LNM. The AUC of model 1, model 2 and model 3 was 0.687, 0.826 and 0.874, and the Delong test showed the AUC of model 3 was significantly higher than that of model 1 and model 2 ($P<0.05$). Decision curve analysis showed that model 3 resulted in a higher degree of net benefit for all the patients than model 1 and model 2.

Conclusion The use of a comprehensive model based on clinicopathology, ultrasound, PET/CT, and PET radiomics can effectively improve the diagnostic efficacy of axillary LNM in BC. Trial registration: This study was registered at ClinicalTrials Gov (number NCT05826197) on 7th, May 2023.

Keywords Breast cancer, Lymph node Metastasis, Radiomics, PET/CT, Ultrasound

*Correspondence:

Xiaoyi Duan

duanxyi@yeah.net

¹PET/CT Center, The First Affiliated Hospital of Xi'an Jiaotong University, 277 Yanta West Road, Xi'an Shaanxi 710061, China



© The Author(s) 2023. **Open Access** This article is licensed under a Creative Commons Attribution 4.0 International License, which permits use, sharing, adaptation, distribution and reproduction in any medium or format, as long as you give appropriate credit to the original author(s) and the source, provide a link to the Creative Commons licence, and indicate if changes were made. The images or other third party material in this article are included in the article's Creative Commons licence, unless indicated otherwise in a credit line to the material. If material is not included in the article's Creative Commons licence and your intended use is not permitted by statutory regulation or exceeds the permitted use, you will need to obtain permission directly from the copyright holder. To view a copy of this licence, visit <http://creativecommons.org/licenses/by/4.0/>. The Creative Commons Public Domain Dedication waiver (<http://creativecommons.org/publicdomain/zero/1.0/>) applies to the data made available in this article, unless otherwise stated in a credit line to the data.

Introduction

BC is a commonly occurring primary malignant tumor in women with high heterogeneity and varying degrees of malignancy [1, 2]. Surgical intervention is essential for its early diagnosis and treatment. The status of axillary LNM is an important factor affecting the prognosis of BC patients [1, 3]. Currently, clinicians mainly rely on mammography, ultrasound, MRI [4] and PET/CT for the diagnosis of axillary LNM in BC [5]. However, the sensitivity or specificity are unsatisfactory [6]. Axillary lymph node biopsy is relatively accurate, but it is an invasive procedure that may cause complications such as lymphedema, pain, numbness, limitation of shoulder movement, and nerve injury [7]. So, a new noninvasive method for pre-operative axillary lymph node assessment is needed. Several studies have demonstrated the potential role of radiomics in the staging, prognosis, and evaluation of BC [8]. Recent studies have shown that radiomics have a good predictive power for evaluating LNM various cancers [9, 10]. Therefore, the study of indirectly evaluating the metastatic status of axillary lymph nodes by extracting the characteristics of breast cancer nodes using radiomics has become a hot topic.

Materials and methods

Study participants

Patients with suspected BC undergoing PET/CT at our hospital, from November 2016 to April 2022, were selected via picture archiving and communication as well as hospital information systems, based on the inclusion process depicted in Fig. 1. This study was conducted in

accordance with the principles of the Declaration of Helsinki and was reviewed and approved by the Medical Ethics Committee of the First Affiliated Hospital of Xi'an Jiaotong University(No. IRB-SOP-AF-16). All data were anonymized prior to analysis. Tumor staging was done in accordance with the eighth edition of the American Joint Committee on Cancer staging manual [11]. This study was funded by the Department of Science and Technology of Shaanxi Province(No. 2023-YBSF-480), and registered with ClinicalTrials.gov (Date of first registration: 24/04/2023, ClinicalTrials.gov Identifier: NCT05826197).

Inclusion criteria: (1) ^{18}F -FDG PET/CT for breast lesions; (2) women with pathologically confirmed BC (age ≥ 18 years); (3) no history of surgery, radiotherapy, or chemotherapy before ^{18}F -FDG PET/CT; and (4) interval between ^{18}F -FDG PET/CT and puncture/surgery ≤ 2 weeks.

Exclusion criteria: (1) multifocal, bilateral, or occult BC; (2) incomplete clinical or pathological data; (3) poor PET/CT image quality preventing automated segmentation of metabolic tumor volume (MTV); and (4) concomitant malignant tumors.

PET/CT imaging methods

PET/CT was performed on all patients using a 64-detector scanner (Gemini TF PET/CT, Philips, Netherlands). ^{18}F -FDG was synthesized by GE MINITRACE mini cyclotron and Tracerlab FX-FDG synthesizer, and the synthetic precursor kit was purchased from ABX, Germany. The synthesized ^{18}F -FDG was released with a purity of $\geq 95\%$, and the quality was assured to be suitable for

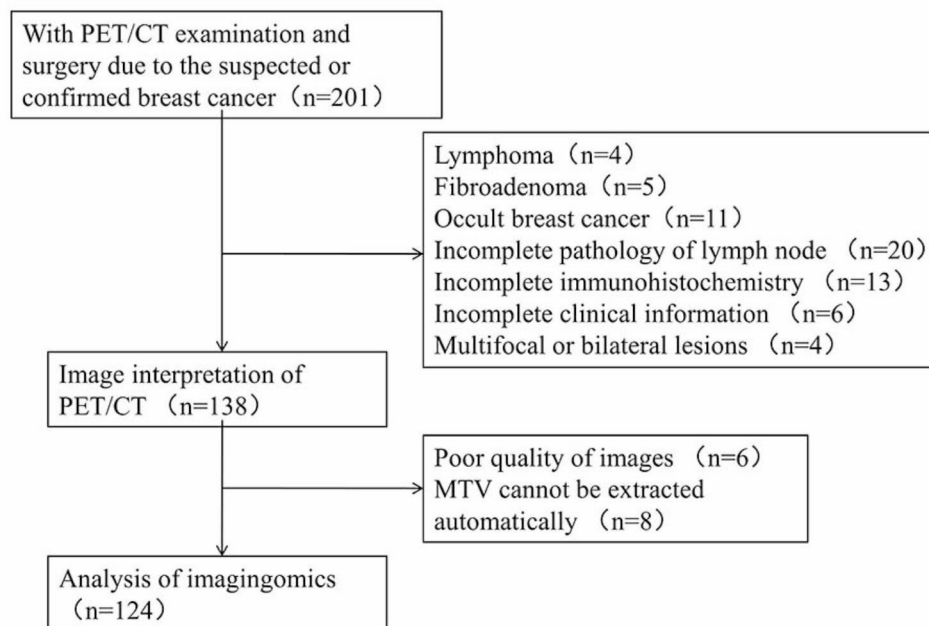


Fig. 1 Study workflow

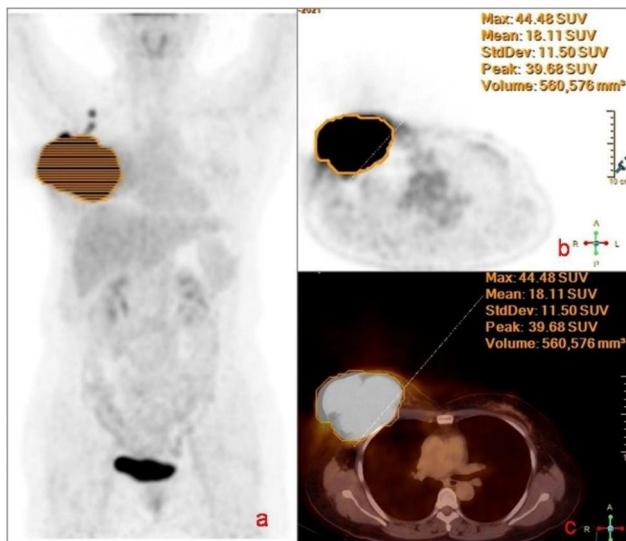


Fig. 2 Metabolic parameters measurements of PET/CT scan. Female, 56 years-old, with BC. MIP image (a) showed the intense uptake of the BC lesion at the right side. The 3D VOI was delineated by physician with the rule of 40% of the maximum standardized uptake value (SUVmax) on the PET image (b) or PET/CT fusion images (c). SUVmax, SUVmean, SD, MTV were measured respectively

human injection. Patients fasted for at least 6 h before injection and had a fasting blood glucose level of less than 12.0 mmol/L. 18 F-FDG (dose 370 MBq/kg) was intravenously injected from the contralateral upper extremity of the affected mammary gland. The patients were encouraged to have sufficient water intake and rest for 60 min. The parameters for the CT scans were as follows: tube voltage 120 kV, tube current 300 mA, layer thickness 5 mm, layer spacing 5 mm, 512×512 matrix. PET collected 7–10 beds with 1.5 min/bed. PET images were corrected by the same machine used for CT data attenuation and reconstructed using an iterative method and time of flight. The imaging data were transferred to a workstation for image post-processing.

Image interpretation

The PET/CT center's chief physician and senior attending physician reviewed the images together and disagreement, if any, was resolved by consensus. The lesion was visually identified. A 3D region of interest (ROI) of the lesion was automatically outlined using the 40% threshold method, and PET metabolic parameters were measured, seen as Fig. 2.

Breast lesions with radionuclide concentrations greater than those in normal breast tissue were considered to be BC lesions, while lymph nodes with radionuclide concentrations greater than those in muscle tissue were considered to be metastatic lymph nodes.

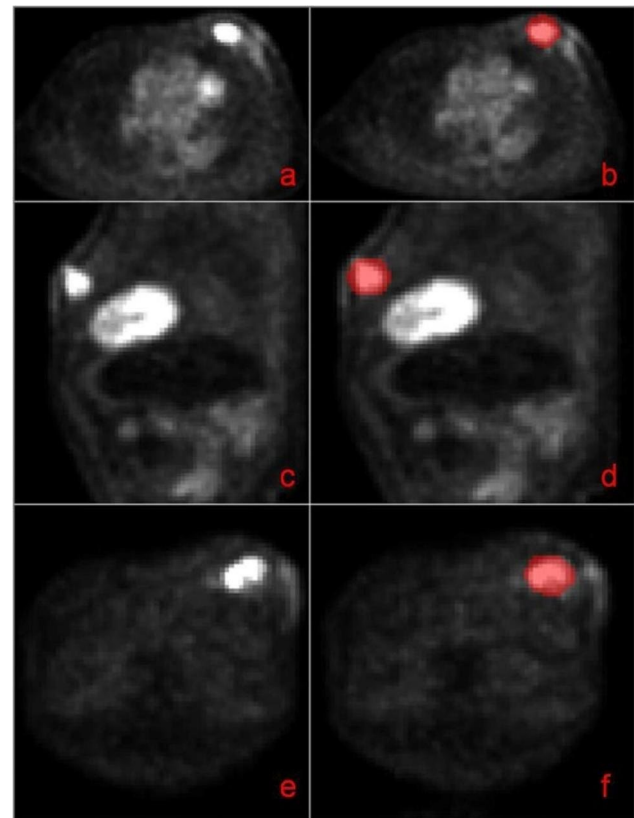


Fig. 3 3D lesion segmentation. Axial (a), sagittal (c), and coronal PET images (e) of breast tumors, outlined axial (b), sagittal (d), and coronal images (f) of tumor ROIs

Radiomics

Image segmentation was performed using ITK-SNAP software [12] (version 3.6.0, <http://www.itksnap.org/>); Brush Style: circular, Brush Size: 10, Brush Options: 3D. The entire tumor volume was outlined on the PET image as ROI for segmentation, seen as Fig. 3. The lesions were marked by the attending physician and checked by the chief physician.

An open source Python package (PyRadiomics version 3.0.1 [13]) was used to extract the radiomics features from the ROI, and a total of 851 radiomics features were finally computed. These features were extracted and defined in accordance with the Image Biomarker Standardization Initiative.

Clinical and pathological features

Breast imaging reporting and data system classification was used to classify all BCs involving lymph nodes. The histological grading of BC was assessed using the internationally accepted Nottingham tissue grading system [14]. BC specimens were fixed in 4% formaldehyde solution and embedded in paraffin wax, sectioned at a thickness of 4 μ m. They were routinely stained with HE and then subjected to immunohistochemistry which included

evaluation of estrogen receptor, progesterone receptor, human epidermal growth factor receptor 2, p53, and cell proliferation nuclear antigen Ki67.

Statistical analysis

Statistical analysis was performed using R language (version 4.1.0, R Foundation for Statistical Computing, Vienna, Austria, URL <https://www.R-project.org/>) and SPSS® (version 25.0, IBM Corp, Armonk, NY, USA) software with a significance level of $\alpha=0.05$. The data obtained were expressed as mean \pm standard deviation. Groups were compared using the independent samples t-test if they were normally distributed with equal variance, otherwise the Mann–Whitney U test was used for comparison. Categorical variables were compared using the χ^2 test or Fisher's exact test. The least absolute shrinkage and selection operator (LASSO) was used to downscale the radiomics features, and the Radiomics Score (RS) was established based on the coefficients of the downscaled features. Univariate and multivariate binary logistic regressions were used to construct three parametric models based on clinicopathology and ultrasound (model 1); clinicopathology, ultrasound, and PET (model 2); and clinicopathology, ultrasound, PET, and radiomics (model 3), for predicting LNM in BC. ROC curves were plotted and area under the curve (AUC) was calculated to evaluate the discrimination of the three models, and the AUCs of the three models were compared using the DeLong test. Furthermore, 1000 bootstraps with put-back repeated sampling were used to internally validate the differentiation of the models and to calculate the corrected AUC. Calibration curves were plotted separately to evaluate the calibration of the three models. The net reclassification index (NRI) and integrated discrimination improvement index (IDII) were used to evaluate the inter-model improvement. Finally, decision curves were plotted to evaluate the net benefit of the three models for all patients.

Results

Comparison of general information

A total of 124 BC patients with a median age of 49 years-old (20–76 years) were included in this study, and the clinic-pathological characteristics of the axillary LNM negative group ($n=89$) and the axillary LNM positive group ($n=35$) were compared to identify potential diagnostic biomarkers of axillary LNM. The T stage, US_BIRADS, US_LNM, and PET_LNM in the positive axillary LNM group was significantly higher than that of in the negative LNM group ($P=0.013$, $P=0.049$, $P<0.001$, $P<0.001$, respectively), seen as Table 1. There were no statistical differences in age, tumor location, quadrant distribution, subtypes, grade, mol-subtypes, SUVmax,

SUVmean, SD and MTV between the two groups ($P>0.05$), as shown in Table 1.

LASSO regression, RS calculation

The radiomics features were normalized using Z-scoring and then downscaled using LASSO regression, and the optimal $\ln\lambda = -2.704$ was determined by cross-validation, as shown in Fig. 4. Based on the linear weighting of the four radiomics features and their coefficients, radiomics score for predicting LNM(RS_LNM) was calculated, that was, $Z_{\text{original_firstorder_10Percentile}} * 0.0891130 + Z_{\text{original_glszm_SizeZoneNonUniformityNormalized}} * 0.2768424 + Z_{\text{waveletLLH_firstorder_Skewness}} * 0.1603961 + Z_{\text{waveletHHH_grrlm_ShortRunEmphasis}} * 0.1117953 - 0.9779143$. RS_LNM for the group of negative LNM and the group of positive LNM were -1.090 ± 0.448 and -0.693 ± 0.344 , respectively, with a statistically significant difference ($t = -4.720$, $P < 0.001$; Fig. 5). In the ROC analysis, the AUC was 0.767 (95% CI: 0.674–0.861; Fig. 6).

Construction and comparison of the three prediction models

The results showed that T stage, US_LNM, and PET_LNM were associated with RS_LNM. Three models with multivariate were constructed for predicting LNM, as shown in Table 2. RS_LNM was an independent predictor when US_LNM and PET_LNM were integrated in the multivariable model, with OR value of 8.078 [95%CI, (1.862–35.050), $P < 0.05$]. The differentiation of the three models was shown in Table 3. The ROC curves showed that model 3 outperformed model 1 for the sensitivity (model 3 vs. model 1, 82.86% vs. 48.57%), and outperformed model 2 for the specificity (model 3 vs. model 2, 82.02% vs. 68.54%). The AUC of model 1, model 2 and model 3 was 0.687, 0.826 and 0.874, seen as Fig. 7, and the DeLong test showed the AUC of model 3 was significantly higher than that of model 1 and model 2, seen as Fig. 8. The nomogram was the visualization of the model 3, seen as Fig. 9.

The calibration curves for all three models showed good calibration, seen as Fig. 10. The continuous NRI for model 2 relative to model 1 was 1.118 (95% CI: 0.797–1.422), $p < 0.001$, and IDII of 0.141 (95% CI: 0.078–0.203), which mean positive improvement. The continuous NRI for model 3 relative to model 2 was 0.666 (95% CI: 0.368–0.963), $p < 0.001$, and IDII of 0.060 (95% CI: 0.007–0.114), $p = 0.026$, which mean improvement.

Decision curve analysis showed that model 2 resulted in a higher degree of net benefit for all the patients than model 1, and model 3 resulted in a higher degree of net benefit for all the patients than model 2, seen as Fig. 11.

Table 1 Comparison of general information of patients in two groups

Parameters	LNM(-) (n = 89)	LNM(+) (n = 35)	t/ χ^2	p
Age	48.33 ± 11.86	51.09 ± 10.62	-1.200	0.232
Tumor location			0.679	0.410
Left	48	16		
Right	41	19		
Quadrant distribution			7.488	0.187
Outer upper	35	13		
Outer lower	11	4		
Inner upper	27	9		
Inner lower	7	0		
Middle upper	3	4		
Middle lower	6	5		
T stage			12.617	0.013
Tis	3	0		
T1	52	10		
T2	26	19		
T3	6	3		
T4	2	3		
Subtypes			1.898	0.387
Invasive ductal carcinoma	77	33		
Invasive lobular carcinoma	9	2		
Ductal carcinoma in situ	3	0		
Grade			1.903	0.386
G1	3	0		
G2	39	13		
G3	47	22		
Mol-subtypes			4.402	0.221
Luminal A	23	6		
Luminal B	27	17		
HER2positive	25	6		
Triple-negative	14	6		
US_BIRADS			9.554	0.049
Bi-rads 1	1	1		
Bi-rads 3	2	1		
Bi-rads 4	55	11		
Bi-rads 5	18	12		
Bi-rads 6	13	10		
US_LNM			20.558	<0.001
negative	79	18		
positive	10	17		
PET_LNM			32.065	<0.001
negative	65	6		
positive	24	29		
SUVmax	7.91 ± 4.46	8.82 ± 5.46	-0.961	0.339
SUVmean	4.22 ± 2.39	4.32 ± 2.4	-0.195	0.846
SD	1.26 ± 0.86	1.44 ± 1.29	-0.909	0.365
MTV	31484.88 ± 153481.91	36169.74 ± 76683.17	-0.172	0.864

Discussion

A large number of clinical data have confirmed that the prognosis of breast cancer patients is closely related to the presence or absence of axillary lymph node metastasis [1, 3]. Traditional imaging methods commonly

used to evaluate the metastatic status of axillary lymph nodes in breast cancer are mostly based on the subjective experience of imaging physicians, semi-quantitative or quantitative analysis of low dimensions, and a lot of deep and high-dimensional data information has not

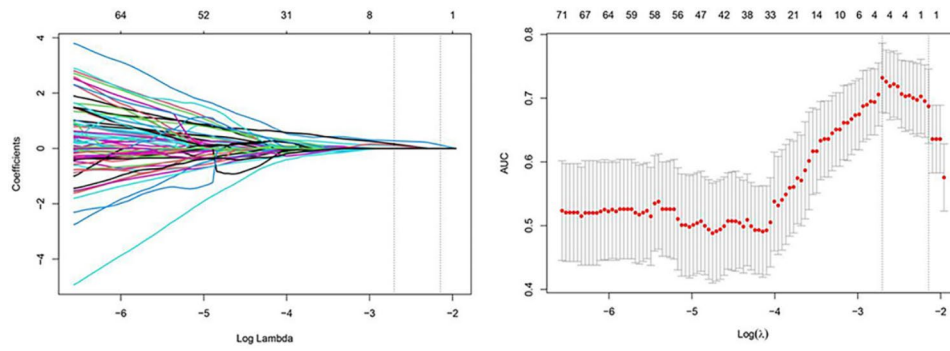


Fig. 4 LASSO regression cross-validation diagram and regression coefficient diagram, the upper horizontal axis is the number of radiomics features corresponding to the models. The two vertical dashed lines in Fig. 4A show the two log (λ) values for minimum mean-squared error minimum and the increase of 1 SD (one standard deviation) mean-squared error minimum determined by cross-validation. Figure 4B shows that with the increase of log (λ), the radiomics features coefficients were gradually compressed to 0, and the number of features was reduced to 4 by the log (λ) with minimum mean-squared error minimum. LASSO, least absolute shrinkage and selection operator

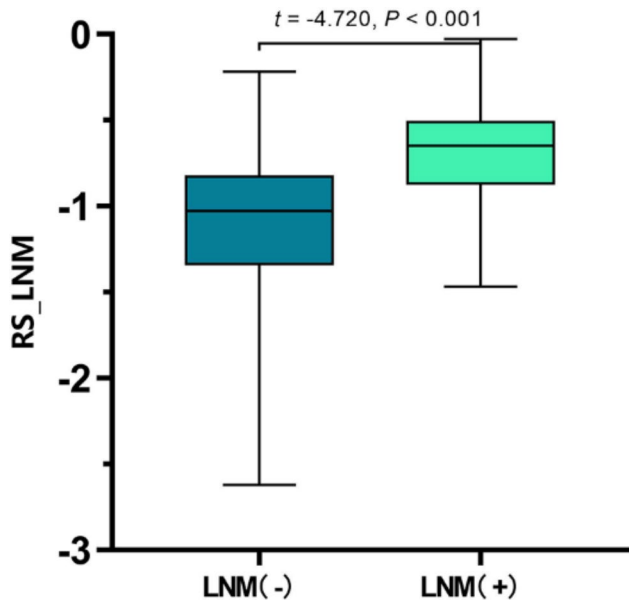


Fig. 5 Comparison of RS_LNM between two groups

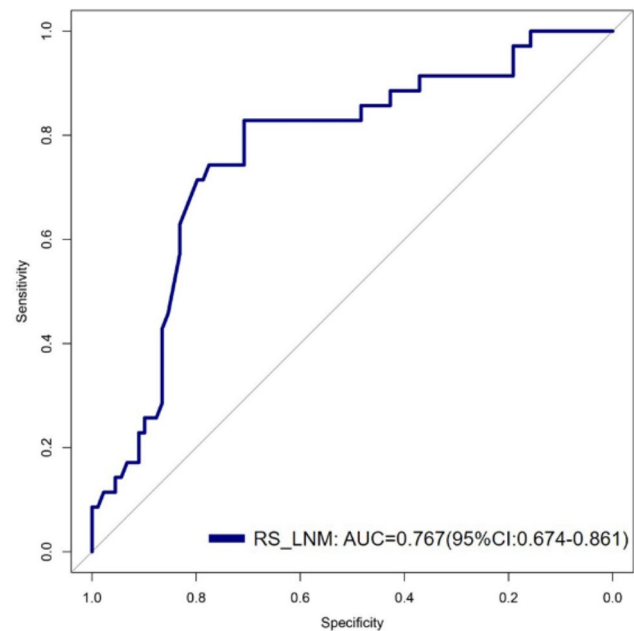


Fig. 6 ROC curve analysis of RS_LNM

Table 2 Multivariate analysis

Parameters	Model 1: T stage + US_LNM		Model 2: T stage + US_LNM + PET_LNM		Model 3: T stage + US_LNM + PET_ LNM + RS_LNM	
	OR(95%CI)	p	OR(95%CI)	p	OR(95%CI)	p
T stage						
US_LNM	7.461(2.932–18.984)	<0.001	4.007(1.407–11.411)	0.009	3.324(1.081–10.217)	0.036
PET_LNM			9.467(3.373–26.572)	<0.001	7.349(2.518–21.448)	<0.001
RS_LNM					8.078(1.862–35.050)	0.005

Table 3 Distinguishability of the three models

Parameters	AUC(95%CI)	p	Cut-off	Se(%)	Sp(%)	Corrected AUC
Model 1	0.687(0.597–0.767)	<0.001	0.19	48.57	88.76	0.686
Model 2	0.826(0.748–0.888)	<0.001	0.07	88.57	68.54	0.823
Model 3	0.874(0.802–0.927)	<0.001	0.28	82.86	82.02	0.864

Note: Corrected AUC by Bootstrap1000

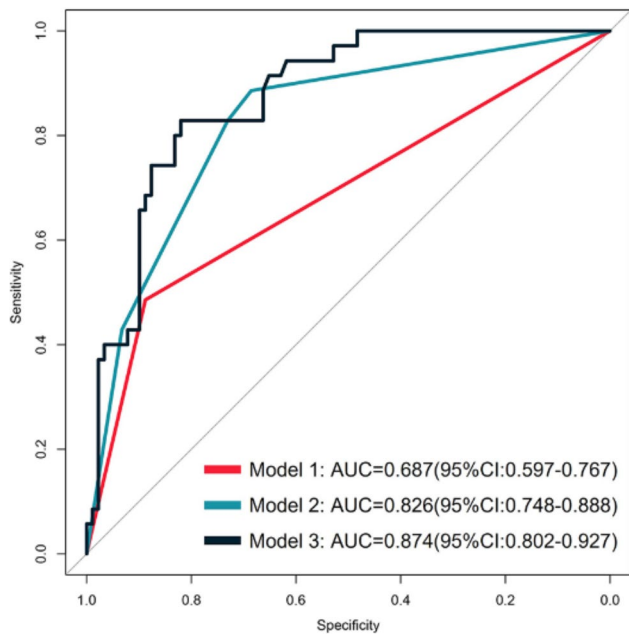


Fig. 7 Comparison of ROC curves for the three models. Model 3 outperformed model 1 for the sensitivity (model 3 vs. model 1, 82.86% vs. 48.57%), and outperformed model 2 for the specificity (model 3 vs. model 2, 82.02% vs. 68.54%)

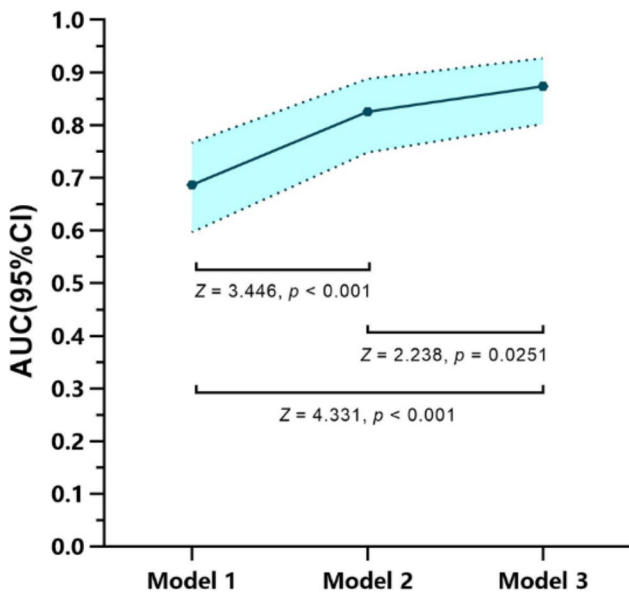


Fig. 8 Pair-wise comparisons of AUC of the three models. The AUCs of model 1, model 2 and model 3 were significantly different

been fully exploited. There is an urgent need for noninvasive methods that can accurately assess axillary LNM in BC patients preoperatively, thereby reducing the need for anterior lymph node biopsy and axillary lymph node dissection. Such noninvasive methods are important for guiding the choice of axillary surgical modality and improving the quality of life of BC patients.

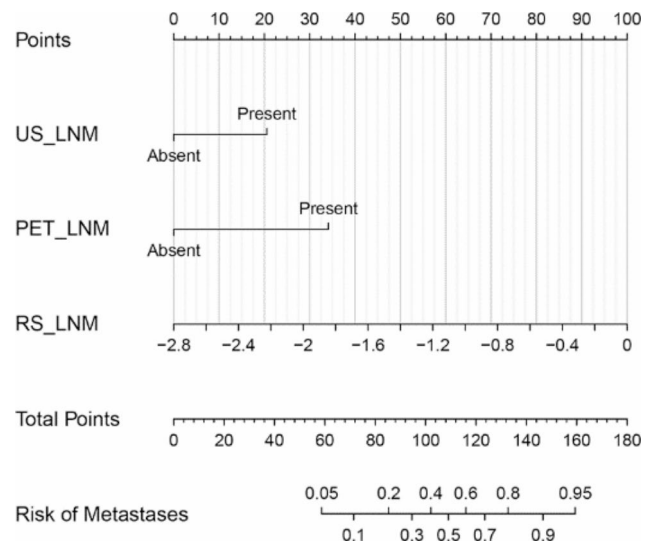


Fig. 9 Nomogram for model 3

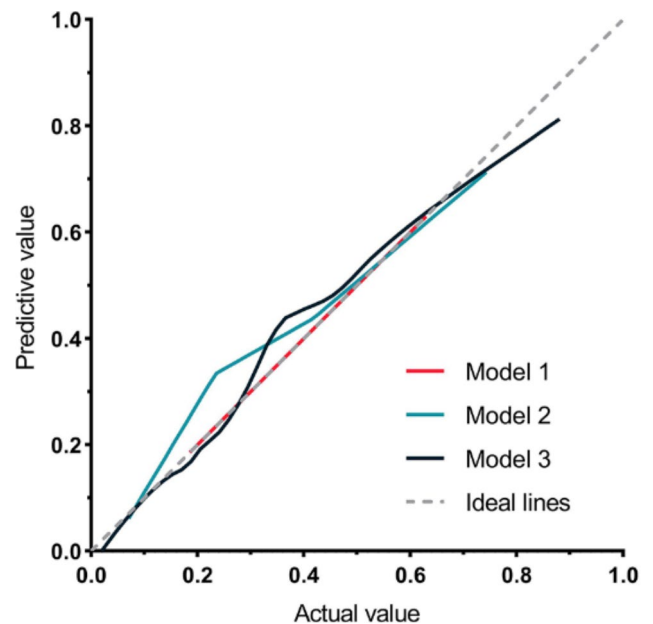


Fig. 10 Calibration curves for the three models

Recent studies have shown that radiomics have a good predictive power for evaluating LNM various cancers [9, 10]. Radiomics features are the product of genotypic and phenotypic influences of tissues that can reflect the biology of tumors [15]. The term “-omics” originated in molecular biology to characterize DNA, RNA, proteins, and metabolites [15]. In medical imaging research, radiomics is the analysis of images to obtain data that may be relevant to clinical outcomes and provide reliable potential imaging-based biomarkers for improving diagnosis, optimizing treatment plans, and predicting outcome [16, 17]. Algorithm-based medical imaging features have the advantages of being

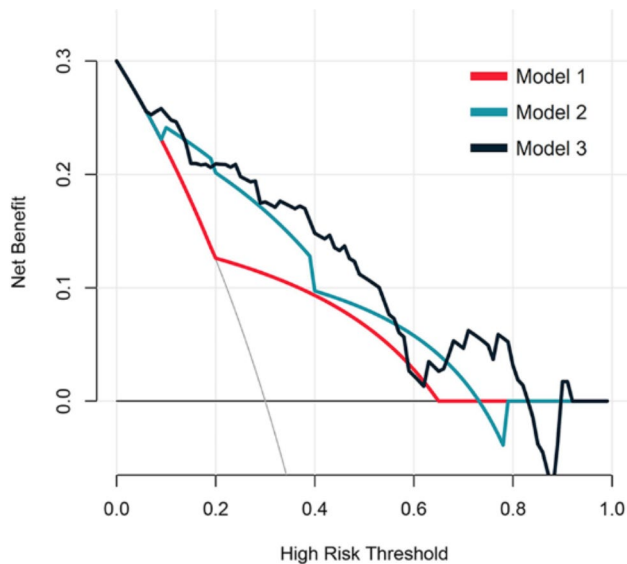


Fig. 11 Decision curves of the three models

non-invasive, sample-independent, real-time, and not limited to the tissues being examined compared to tissue-based biomarkers. The current approach of predicting axillary LNM in BC using radiomics evaluates the axillary lymph node images obtained by X-ray mammography, ultrasound, and MRI, of which evaluation of the ultrasound scans are the most frequently used for diagnosis. Mao et al. [18] predicted axillary LNM based on mammography radiomics with an AUC of 0.79; Qiu et al. [19] predicted axillary LNM based on breast ultrasound radiomics with an AUC of 0.759; and Tan et al. [20] predicted axillary LNM based on breast MRI radiomics with an AUC of 0.805. Lee et al. [21] and Gao et al. [22] achieved good predictive results based on breast ultrasound radiomics to evaluate axillary LNM.

Studies have demonstrated the potential application of PET radiomics in the diagnosis, staging, and assessment of treatment response in breast cancer [8]. The application of PET radiomics has not been widely studied in the diagnosis of BC LNM; however, it has shown to improve the diagnostic sensitivity for LNM patients with BC [23]. As a non-invasive, visual method that can quantify the entire tumor heterogeneity, PET radiomics can reflect the biological characteristics of tumors more objectively and comprehensively by extracting quantifiable image features from the ROI of PET images in high throughput, creating high-dimensional datasets, and mining the features associated with tumors through data mining analysis techniques [24]. In previous studies [22, 23], PET imaging-based histology of primary BC was analyzed to predict axillary lymph node status with AUCs of 0.64 and 0.89, respectively, thus showing a large difference in diagnostic efficacy. Therefore, in this study, a comprehensive model (model 3) was constructed to predict axillary

LNM based on PET radiomics in addition to the evaluation of the clinical, pathological, ultrasound, and PET/CT parameters. The results showed that model 3 had higher a discrimination and calibration for predicting LNM in BC, with positive improvements in both continuous NRI and IDII, relative to the other two models. Model 3 had a stronger predictive performance as well as a net benefit for more patients.

Previous studies have often predicted LNM by the volume of the primary tumor and its metabolic parameters. For example, studies by De [25] and Song et al. [5, 26] showed that the metabolic activity of the primary tumor obtained by 18 F-FDG PET/CT in rectal, gastric, and BCs was positively correlated with LNM. In contrast, SUVmax, SUVmean, SD, and MTV did not significantly correlate with axillary LNM the present study. Another study [23] showed that data on pathological classification, molecular subtypes, and immunohistochemistry were not associated with axillary LNM, and the present study was similar to these results.

Limitations of this study are that it was a retrospective single-center study with possible selection bias; patients with multifocal lesions, bilateral lesions, and occult lesions were excluded because it was difficult to identify lesions that would lead to LNM; and only internal validation was performed due to the volume of data, which needs to be expanded for external validation.

Conclusion

In this study, a comprehensive model to diagnose axillary LNM was constructed based on clinicopathology, ultrasound, PET/CT, and PET radiomics. This model with a high sensitivity (82.86%), specificity (82.02%), and an AUC of 0.874 can achieve a non-invasive, individualized, precise, and holistic presurgical assessment of axillary LNM in BC patients. Further controlled prospective studies are needed to validate the predictive accuracy of this comprehensive model.

Abbreviations

LNM	Lymph Node Metastasis
BC	Breast Cancer
18 F-FDG	18 F-fluorodeoxyglucose
MTV	Metabolic Tumor Volume
ROI	Region of Interest
SUV	Standardized Uptake Value
LASSO	Least Absolute Shrinkage and Selection Operator
RS	Radiomics Score
AUC	Area Under the Curve
NRI	Net Reclassification Index
IDII	Integrated Discrimination Improvement

Acknowledgements

Not applicable.

Author contributions

Yan Li and Dong Han are co-first author. Yan Li, Dong Han and Xiaoyi Duan contributed to the conception of the study; Yan Li and Cong Shen, performed the experiments; Yan Li, Cong Shen and Dong Han contributed significantly

to analysis and manuscript preparation; Yan Li, Dong Han and Xiaoyi Duan helped perform the analysis with constructive discussions.

Funding

This study was funded by the Department of Science and Technology of Shaanxi Province (No. 2023-YBSF-480).

Data Availability

We confirm that all the materials and data with regard to the analysis in the manuscript are available for request. Please contact Yan Li for data request.

Declarations

Competing interests

The authors declare no competing interests.

Clinical trials

Date of first registration: 24/04/2023.

ClinicalTrials.gov Identifier: NCT05826197.

Ethics approval and consent to participate

This study was approved by the Ethics Committee of the First Affiliated Hospital of Xi'an Jiaotong University (No. IRB-SOP-AF-16). Written informed consent for publication was obtained from all participants.

Consent for publication

Not Applicable.

Received: 7 July 2023 / Accepted: 9 October 2023

Published online: 24 October 2023

References

- Siegel RL, Miller KD, Fuchs HE, et al. Cancer statistics, 2022. *CA Cancer J Clin.* 2022;72(1):7–33.
- Siegel RL, Miller KD, Jemal A. Cancer statistics, 2023. *CA Cancer J Clin.* 2023;73(1):17–48.
- Islami F, Sauer AG, Kimberly D, Miller, et al. Proportion and number of cancer cases and deaths attributable to potentially modifiable risk factors in the United States. *CA Cancer J Clin.* 2018;68(1):31–54.
- Calabrese A, Santucci D, Landi R, et al. Radiomics MRI for lymph node status prediction in Breast cancer patients: the state of art. *J Cancer Res Clin Oncol.* 2021;147(6):1587–97.
- Song BI, Kim HW, Won KS. Predictive value of. *Ann Surg Oncol.* 2017;24(8):2174–81.
- Kasem J, Wazir U, Mokbel K, et al. Sensitivity, specificity and the diagnostic accuracy of PET/CT for Axillary staging in patients with stage I-III Cancer: a systematic review of the literature. *In Vivo.* 2021;35(1):23–30.
- Liang Y, Chen XS, Tong YW, et al. Higher axillary lymph node Metastasis burden in Breast cancer patients with positive preoperative node biopsy: may not be appropriate to receive sentinel lymph node biopsy in the post-ACOSOG Z0011 trial era. *World J Surg Oncol.* 2019;17(1):37.
- Luca Urso, Luigi Manco, Angelo Castello, et al. PET-derived radiomics and artificial intelligence in breast cancer: a systematic review. *Int J Mol Sci.* 2022; 23(21):13409.
- Cai D, Duan X, Wang W, et al. A metabolism-related radiomics signature for predicting the prognosis of Colorectal cancer. *Front Mol Biosci.* 2021;7:613918.
- Wang X, Zhao X, Li Q, et al. Can peritumoral radiomics increase the efficiency of the prediction for lymph node Metastasis in clinical stage T1 lung adenocarcinoma on CT? *Eur Radiol.* 2019;29(11):6049–58.
- Giuliano AE, Connolly JL, Edge SB, et al. Breast Cancer-major changes in the American Joint Committee on Cancer eighth edition cancer staging manual. *CA Cancer J Clin.* 2017;67(4):290–303.
- Paul A, Yushkevich J, Piven HC, Hazlett et al. User-guided 3D active contour segmentation of anatomical structures: significantly improved efficiency and reliability. *Neuroimage.* 2006;31(3):1116–28.
- Joost JM, van Griethuysen A, Fedorov C, Parmar, et al. Computational Radiomics System to Decode the Radiographic phenotype. *Cancer Res.* 2017;77(21):e104–7.
- Cipolla V, Santucci D, Guerrieri D, et al. Correlation between 3T apparent diffusion coefficient values and grading of invasive breast carcinoma. *Eur J Radio.* 2014;83(12):2144–50.
- Valdora F, Houssami N, Rossi F, et al. Rapid review: radiomics and Breast cancer. *Breast Cancer Res Treat.* 2018;169(2):217–29.
- Yu Y, He Z, Ouyang J, et al. Magnetic resonance imaging radiomics predicts preoperative axillary lymph node Metastasis to support surgical decisions and is associated with Tumor microenvironment in invasive Breast cancer: a machine learning, multicenter study. *EBioMedicine.* 2021;69:103460.
- Feng Q, Hu Q, Liu Y, et al. Diagnosis of triple negative Breast cancer based on radiomics signatures extracted from preoperative contrast-enhanced chest computed tomography. *BMC Cancer.* 2020;20(1):579.
- Mao N, Yin P, Li Q, et al. Radiomics nomogram of contrast-enhanced spectral mammography for prediction of axillary lymph node Metastasis in Breast cancer: a multicenter study. *Eur Radiol.* 2020;30(12):6732–9.
- Qiu X, Jiang Y, Zhao Q, et al. Could ultrasound based radiomics noninvasively predict axillary lymph node Metastasis in Breast cancer? *J Ultrasound Med.* 2020;39(10):1897–905.
- Tan HN, Gan FW, Wu YP, et al. Preoperative prediction of Axillary Lymph Node Metastasis in breast carcinoma using Radiomics features based on the Fat-suppressed T2 sequence. *Acad Radiol.* 2020;27(9):1217–25.
- Lee SE, Sim Y, Kim S, et al. Predictive performance of ultrasonography-based radiomics for axillary lymph node Metastasis in the preoperative evaluative of Breast cancer. *Ultrasonography.* 2021;40(1):93–102.
- Gao Y, Luo Y, Zhao C, et al. Nomogram based on radiomics analysis of primary Breast cancer ultrasound images: prediction of axillary lymph node Tumor burden in patients. *Eur Radiol.* 2021;31(2):928–37.
- Song BI. A machine learning based radiomics model for the prediction of axillary lymph node Metastasis in Breast cancer. *Breast Cancer.* 2021;28(3):664–71.
- Cook GJR, Azad G, Owczarczyk K, et al. Challenges and promises of PET radiomics. *Int J Radiat Oncol Biol Phys.* 2018;102(4):1083–9.
- De Nardi P, Guarneri G, Canevari C, et al. Prognostic value of fluorodeoxyglucose positron emission tomography/computed tomography and inguinal sentinel lymph node biopsy in patients with anal cancer. *Colorectal Dis.* 2019;21(9):1017–24.
- Song BI. Nomogram using F-18 fluorodeoxyglucose positron emission tomography /computed tomography for preoperative prediction of lymph node Metastasis in gastric cancer. *World J Gastrointest Oncol.* 2020;12(4):447–56.

Publisher's Note

Springer Nature remains neutral with regard to jurisdictional claims in published maps and institutional affiliations.